

# PHOTONICS Research

## Scalable cyclic transformation of orbital angular momentum modes based on a nonreciprocal Mach–Zehnder interferometer

YU-FANG YANG,<sup>1,†</sup> MING-YUAN CHEN,<sup>1,†</sup> FENG-PEI LI,<sup>1</sup> YA-PING RUAN,<sup>1</sup> ZHI-XIANG LI,<sup>1</sup> MIN XIAO,<sup>1,2</sup> HAN ZHANG,<sup>1,3,4</sup> AND KE-YU XIA<sup>1,3,5</sup>

<sup>1</sup>National Laboratory of Solid State Microstructures, School of Physics, College of Engineering and Applied Sciences, and Collaborative Innovation Center of Advanced Microstructures, Nanjing University, Nanjing 210093, China

<sup>2</sup>Department of Physics, University of Arkansas, Fayetteville, Arkansas 72701, USA

<sup>3</sup>Hefei National Laboratory, Hefei 230088, China

<sup>4</sup>e-mail: zhanghan@nju.edu.cn

<sup>5</sup>e-mail: keyu.xia@nju.edu.cn

<sup>†</sup>These authors contributed equally to this work.

Received 12 April 2024; revised 19 July 2024; accepted 27 July 2024; posted 29 July 2024 (Doc. ID 526115); published 30 September 2024

The orbital angular momentum (OAM) of photons provides a pivotal resource for carrying out high-dimensional classical and quantum information processing due to its unique discrete high-dimensional nature. The cyclic transformation of a set of orthogonal OAM modes is an essential building block for universal high-dimensional information processing. Its realization in the quantum domain is the universal quantum Pauli-X gate. In this work, we experimentally demonstrate a cyclic transformation of six OAM modes with an averaged efficiency higher than 96% by exploiting a nonreciprocal Mach–Zehnder interferometer. Our system is simple and can, in principle, be scaled to more modes. By improving phase stabilization and inputting quantum photonic states, this method can perform universal single-photon quantum Pauli-X gate, thus paving the way for scalable high-dimensional quantum computation. © 2024 Chinese Laser Press

<https://doi.org/10.1364/PRJ.526115>

### 1. INTRODUCTION

It is well known that the Laguerre–Gaussian (LG) mode of a light beam carries a helical phase term of  $\exp(i/l\theta)$ , where  $\theta$  is the azimuthal angle and  $l$  is the topological charge, indicating the orbital angular momentum (OAM) of photons. Each photon has a well-defined OAM of  $l\hbar$  [1]. The OAM of photons provides high discrete dimensions for encoding information. Thus, it becomes a promising candidate for high-dimensional information processing. For this reason, it has been widely used in numerous classical [2–4] and quantum communication protocols [5–8], two-photon quantum entanglement in a high-dimensional Hilbert space [9–13], and multi-photon entanglement [14–16].

Unitary transformations leveraging the OAM of photons play the central roles in high-dimensional information technologies. Classical transformation between high-order LG and Hermite–Gaussian (HG) modes has been performed by correctly arranging the cylindrical lenses [17]. Recently, a classical four-mode cyclic transformation has been first realized by using OAM beam splitter (OAM-BS) modules [18], which are the Mach–Zehnder interferometers (MZIs) built from beam splitters (BSs) and Dove prisms. The principle of classical cyclic

transformation has been extended to accomplish a four-dimensional Pauli-X gate by adding a phase-locking system and utilizing the quantum tomography technique [19]. Subsequently, a five-dimensional Pauli-X gate is implemented by modulating the wavefront of the OAM beam through the wavefront matching technique [20]. Multi-mode cyclic transformation based on the OAM beams is the basis for the high-dimensional Pauli-X gates. Arbitrary unitary transformation for single photons can be achieved by the combination of high-dimensional Pauli-X and Pauli-Z gates [21]. The high-dimensional Pauli-Z gate is simply realized by using a Dove prism [22]. However, both classical cyclic transformation and quantum Pauli-X gates are limited up to five modes thus far. It is highly desirable to extend unitary transformations to more modes in the OAM-mode basis.

To leverage the OAM of photons for high-dimensional information processing, it is crucial to spatially separate the OAM modes. A variety of schemes are proposed to accomplish this task [23–30]. Among these methods, the OAM-BS module achieves great success. It can separate the odd and even OAM modes [23,24]. Zhang *et al.* improved this OAM-BS module by replacing the BSs with polarization beam splitters

(PBSs) and separated the OAM modes [25]. To apply this module to a large number of modes, multiple MZIs need to be cascaded [26]. This greatly increases the experimental complexity and reduces the reliability and the fidelity. It remains a challenge to conduct many-mode unitary transformations without considerably adding the system complexity. The FP cavity has been used to sort the OAM modes [30]. It is yet to be exploited for high-dimensional unitary transformations.

In this work, we experimentally realize a six-mode cyclic transformation with an efficiency larger than 96% by building a nonreciprocal MZI. This MZI leverages the nonreciprocal control of the optical circulator and as an OAM filter. Our scheme can be generalized to higher dimensions by only adjusting the cavity parameters, without the need to add additional optical components.

The paper is organized as follows. In Section 2, we explain the concept and the system for the high-dimensional cyclic transformation based on photonic OAMs. Then, the experimental setup is shown in Section 3. In Section 4, we demonstrate the performance of the proposed cyclic transformation by using six OAM modes as an example. In the end, we summarize the results and discuss the potential applications of our scheme.

## 2. SYSTEM AND CONCEPT

A classical cyclic transformation and the quantum Pauli-X gate encoded in a high-dimensional OAM basis perform the conversion of  $(|-(l+1)\rangle, |-l\rangle, \dots, |l-1\rangle, |l\rangle) \rightarrow (|-l\rangle, |-(l-1)\rangle, \dots, |l\rangle, |-(l+1)\rangle)$ . Figure 1(a) conceptually depicts

our method using a nonreciprocal MZI for implementing a high-dimensional cyclic transformation and Pauli-X gate. The nonreciprocal MZI consists of two optical circulators, two identical FP cavities, and an OAM flipper. To conduct cyclic transformation, we input a vortex OAM mode of light beam for the cyclic transformation or the single-photon superposition state of OAM modes for the Pauli-X gate. A spiral phase plate (SPP) is used to convert the  $l$ th OAM mode of the input field to the  $(l+1)$ th mode. As demonstrated in Ref. [30], the resonance frequency of an FP cavity is crucially dependent on the absolute value of the topological charge  $|l|$  of the OAM mode. The key idea of our method leverages this  $l$ -dependent nature of an FP cavity and the nonreciprocal light modulation of an optical circulator. In our arrangement, the FP cavity is resonant with the highest-order  $(l+1)$ th mode but largely detuned with other modes. It transmits the on-resonance  $(l+1)$ th mode but reflects other off-resonance modes. In the ideal case, the spectrum of the input field is well within the linewidth of the FP cavity. The transmission and reflection are nearly unity; see Fig. 1(b). However, the transmitted and reflected fields keep their phases unchanged; see Fig. 1(c). With the first pair of the circulator (C1) and the FP cavity (FP1), the reflected modes are led to the second circulator (C2). The OAM of the transmitted field of the FP1 is first flipped and then incident to the second FP cavity (FP2), which is assumed identical with the FP1. This flipper is used for converting the transmitted  $(l+1)$ th mode to the  $-(l+1)$ th input mode. This flipper can also be inserted into another arm of the MZI. Then, the field transmits the FP2. The modes

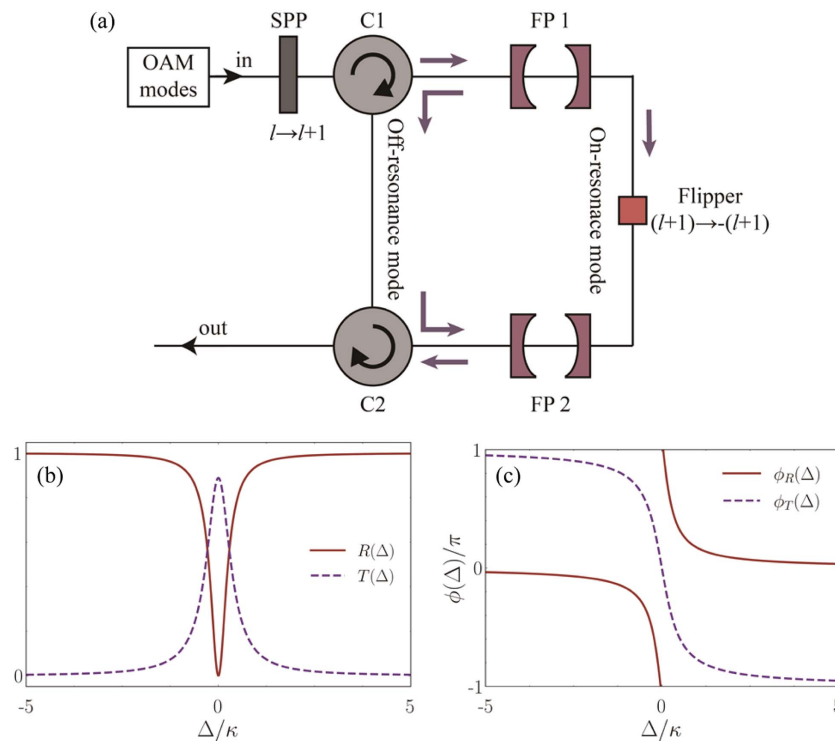


**Fig. 1.** (a) Conceptual diagram for cyclic transformation of OAM modes and the high-dimensional Pauli-X gate based on a nonreciprocal MZI. An SPP increases the topological charge of an OAM mode by one to the input  $l$ th mode. Optical circulators are used to redirect light reflected off the FP cavity to the third path. This FP cavity transmits the selected OAM mode but reflects other modes. A flipper is used to convert the transmitted  $(l+1)$ th mode to the  $-(l+1)$ th one. (b) Reflection and transmission spectra of the FP cavity. (c) Phases of the reflected and transmitted fields.

reflected off the FP1 are input to the FP2 via the C2 and then reflected again by the FP2. The overall reflected fields and the transmitted field are combined with the C2 as the final output. Thus, we can perform the high-dimensional classical cyclic transformation and the quantum Pauli-X gate with this non-reciprocal MZI forming with these two pairs of the circulators and the FP cavities.

Below we provide an explanation for the  $l$ -dependent transmission and reflection of the FP cavity. The transverse distribution of the LG mode in the FP cavity is given in cylindrical coordinates under the paraxial approximation by [1]

$$u_{pl}(r, \theta, z) = \frac{C}{\sqrt{1 + z^2/z_R^2}} \left[ \frac{\sqrt{2}r}{w(z)} \right]^l L_p^l \left[ \frac{2r^2}{w(z)^2} \right] \exp \left[ \frac{-r^2}{w(z)^2} \right] \times \exp \left[ \frac{-ikr^2 z}{2(z^2 + z_R^2)} \right] \exp(-il\theta) \times \exp[i(2p + |l| + 1)\psi(z)]. \quad (1)$$

In the above equation,  $C$  is a normalization constant,  $z_R$  is the Rayleigh range of the beam,  $w(z)$  is the radius of the beam, and  $L_p^l$  is the generalized Laguerre-Gauss polynomial with azimuthal and radial mode indices  $l$  and  $p$ , respectively. The term  $\psi(z) = \arctan(z/z_R)$  is the Gouy phase. The above equation implies that higher-order LG modes have an additional Gouy phase shift with respect to the Gaussian beam. This Gouy phase is attributed to the increased transverse structure of the beam. It enables us to separate out the different OAM modes by using the FP cavity. Based on this phase shift and the standing wave condition of the cavity, the resonance condition of the FP cavity can be written as [30]

$$\omega = \frac{\pi c}{D} \left[ q + (2p + |l| + 1) \frac{\phi}{\pi} \right], \quad (2)$$

where  $D$  is the distance between the front and rear mirrors of the FP cavity,  $q$  is an integer, and the accumulated Gouy phase shift of the LG modes is  $\phi = \arccos\{\pm[(1 - D/R_1) \cdot (1 - D/R_2)]^{1/2}\}$  when the light beam travels from one end of the cavity to the other. It is determined by the mirror curvatures ( $R_1$  and  $R_2$ ). For a fixed cavity length  $D$ , the LG modes clearly exhibit distinct resonant frequencies dependent on  $|l|$ .

Exploiting the Gouy-phase-induced frequency splitting, we can filter a selective OAM mode with an FP cavity. For a two-sided FP cavity, the cavity reflection and transmission coefficients can be derived from the input-output relation

$$r(\Delta) = 1 - \frac{2\kappa_l}{i\Delta + \kappa}, \quad (3a)$$

$$t(\Delta) = \frac{2\sqrt{\kappa_l \kappa_r}}{i\Delta + \kappa}. \quad (3b)$$

Here,  $\Delta = \omega - \omega_c$  is the detuning between the input LG modes and the cavity resonance frequency. The decays caused by the left and right mirrors have the rates  $\kappa_l$  and  $\kappa_r$ , respectively. According to our experiment, we can assume  $\kappa_l = \kappa_r$ . The total decay rate of the cavity is denoted as  $\kappa \equiv \Delta\omega$ . The reflection and transmission spectra of the FP cavity can then be expressed as  $T(\Delta) = |t(\Delta)|^2$  and  $R(\Delta) = |r(\Delta)|^2$ . They are shown in Fig. 1(b). The reflected and transmitted photons also

suffer to an additional scattering phase shift, which is  $\phi_R(\Delta) = \text{Arg}[r(\Delta)]$  and  $\phi_T(\Delta) = \text{Arg}[t(\Delta)]$ , respectively, where the function  $\text{Arg}[x]$  means the phase of a complex number  $x$ . The phase shifts versus detuning are plotted in Fig. 1(c). It can be found from Figs. 1(b) and 1(c) that the selected resonant LG mode directly passes through the cavity with zero scattering phase, while other off-resonance OAM modes are completely reflected off the cavity without phase change. Thus, the resonant OAM mode is separated/filtered by the FP cavity. There is no additional phase introduced among the OAM modes. This nature of the transmission and reflection of the FP cavity meets the key requirement of a high-dimensional X-gate: the relative phase of an input state in superposition needs to remain unchanged in the ideal case.

Experimentally, we can choose the  $(l + 1)$ th OAM mode resonant with the FP cavity by adjusting the cavity length  $D$ . Other involved OAM modes are reflected off the FP cavity and then are directed to another path.

### 3. EXPERIMENTAL SETUP

Here, we give an experimental demonstration of six-mode cyclic transformation using the above system and concept. The experimental setup is depicted in Fig. 2. It is composed of three parts: OAM-mode preparation, cyclic transformation, and OAM-mode measurement.

In the OAM-mode preparation section, the incident laser beam is a horizontally polarized zeroth-order Gaussian beam with the wavelength locked at 794.9693 nm. The Q-plate (QP) is a birefringent waveplate with spatially varying optical axis orientation that can only modulate the phase of the beam [31]. A sandwich combination composed of two quarter-wave plates (QWPs) and one QP is equivalent in principle to one SPP. It can transform the zeroth-order Gaussian mode into an arbitrary higher-order LG mode without changing the polarization state. After passing through the first QWP-QP-QWP combination, the Gaussian beam is transformed

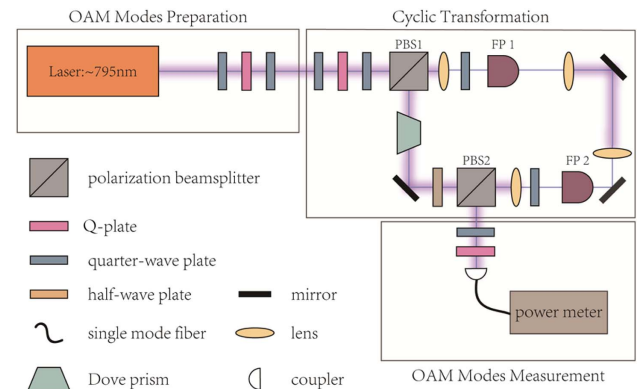


**Fig. 2.** Schematic of the experimental setup. The light source is a DL pro single-frequency continuous laser. A polarization beam-splitter (PBS) and a QWP form an optical circulator, which is used to redirect light reflected off the FP cavity to the third path [30]. The incident light is horizontally polarized. Light reflected by the FP1 (FP2) cavity passes the QWP twice, transforming into the vertically polarized light, and therefore exits at the reflective end of the PBS1 (PBS2). The thicker purple lines indicate the collimated laser beams.

into an OAM beam with an azimuthal mode index of  $l = -3, -2, -1, 0, 1, 2$ .

After the OAM mode enters the cyclic transformation section, it goes through the second QWP–QP–QWP combination to shift to  $(l + 1)$ th mode, where  $q = 1/2$  for QP. The OAM modes become the modes  $\{l = -2, -1, 0, 1, 2, 3\}$ . The FP1 and FP2 cavities are used as the OAM-mode separator and combiner, respectively. We experimentally adjust the length of the FP1 and FP2 cavities via temperature controllers so that the selected  $l = 3$  mode is resonantly transmitted. Other modes with  $l \neq 3$  are off-resonance with the cavities and thus reflected. The mode of  $l = 3$  propagates in the right arm embedded with the FP cavities. It is reflected by two mirrors and then transmits the FP2 cavity. Finally, it exits the right arm of the MZI after being reflected by the PBS2. Note that each reflection flips the OAM quantum number  $l$ . The third OAM mode is reflected odd (three) times. As a result, it changes to the mode with  $l = -3$ . Other OAM modes with  $l \neq 3$  are reflected off the FP1 and FP2 cavities. The reflection of the cavity does not accumulate a phase shift to the OAM modes, as discussed earlier. We use the PBS and a quarter-wave plate to form an optical circulator. The lens right to the PBS is used to adjust the waist of the laser beams. The fields reflected off the FP1 are first directed by the first circulator into the left arm. A Dove prism is embedded into this arm and works as an OAM flipper. It adds one more OAM flipping to the off-resonant modes in order to ensure that the off-resonant modes in the left arm of the MZI have an even number of reflections, while the resonant mode in the right arm of the MZI has an odd number of reflections. The fields transmit the second circulator, are reflected off the FP2, and then are redirected to the photodetector with the selected OAM mode from the right arm. After these processes, the input OAM modes  $\{-3, -2, -1, 0, 1, 2\}$  are finally transformed to  $\{-2, -1, 0, 1, 2, -3\}$  after passing through the cyclic transformation module. A cyclic transformation based on the OAM modes is realized.

In the OAM-mode measurement section, a set of QWP and QP is used to convert the higher-order LG modes into the zeroth-order Gaussian mode, which are then collected through single-mode fiber and detected by power meter.

#### 4. EXPERIMENTAL RESULTS AND DISCUSSION

In Eq. (1), the electric field of the LG mode at its waist plane ( $z = 0$ ) can be described as follows [32]:

$$u_{p,l}(r, \theta) = \sqrt{\frac{2p!}{\pi w_0^2 (p + |l|)!}} \left(\frac{\sqrt{2}r}{w_0}\right)^{|l|} L_p^{|l|} \left(\frac{2r^2}{w_0^2}\right) \times \exp\left(\frac{-r^2}{w_0^2}\right) \exp(-il\theta), \quad (4)$$

where  $w_0$  is the radius of the zeroth-order Gaussian beam at the waist. When the incident light beam is in the zeroth-order Gaussian mode, the QP can only modulate its phase to generate a vortex beam, which is a special case of hypergeometric Gaussian beam [33]. Thus, the created beam is expressed as

$$U_l(r, \theta) = \exp\left(\frac{-r^2}{w_0^2}\right) \exp(-il\theta). \quad (5)$$

The hypergeometric Gaussian beam can be expanded as a superposition of LG modes with same topological charge  $l$ , and they can be written as

$$U_l(r, \theta) = \sum_p C_p u_{p,l}(r, \theta). \quad (6)$$

Here the probability amplitude  $C_p$  is given by [32]

$$C_p = \sqrt{\frac{(p + |l|)!}{p!}} \frac{\Gamma\left(p + \frac{|l|}{2}\right) \Gamma\left(\frac{|l|}{2} + 1\right)}{\Gamma\left(\frac{|l|}{2}\right) \Gamma(p + |l| + 1)}, \quad (7)$$

where  $\Gamma(x)$  is the gamma function. The weightings of the fundamental radial mode ( $p = 0$ ) decrease dramatically with increasing  $l$  mode. The energy gradually shifts to higher-order radial modes ( $p \neq 0$ ). The FP cavities have the identical resonance point for the same value of  $2p + |l|$  but different values of  $p, l$ . This situation affects the accuracy of the cyclic transformation results. Thus, the weighting of the radial mode ( $p = 0$ ) needs to be increased for a given higher-order  $l$  mode. We use the lens to adjust the waist size of the incident light beam entering the FP1 cavity. As suggested by Ref. [34], the energy content in the radial mode ( $p = 0$ ) can be significantly improved when  $w'_0 = w_0/\sqrt{|l| + 1}$ , and in turn, the transmission of the higher-order  $l$  mode is the highest. For example, when the beam waist of the FP1 cavity is  $50 \mu\text{m}$ , the beam waist of the incident light beam with  $l = \pm 3$  modes needs to match the cavity beam waist, so that  $w_0 = 50 \mu\text{m}$ . The lens is adjusted to reduce the beam waist of the incident vortex beam to  $w'_0 = 25 \mu\text{m}$ . As shown in Fig. 3(a), for two different beam waist sizes of the incoming beam, the transmission of the FP1 cavity in different  $l$  modes is measured. The measured data imply that reducing the beam waist to the optimal condition  $w'_0 = w_0/2$  significantly increases the transmission of all the higher-order  $l$  modes. Further reduction of the beam waist does not enhance the transmission of the FP cavities.

Experimentally, both FP1 and FP2 cavities are plano-convex lenses composed of monolithic fused silica crystal with 90% reflectance on both planar and convex surfaces. The convex surface of the lenses has a curvature radius of 25 mm. We mounted the lenses on copper blocks. The copper block is placed on a thermoelectric cooler. A temperature controller is utilized to control the temperature of the copper block. The temperature stability of FP cavities is less than  $0.01^\circ\text{C}$  for 24 h. The stabilized temperature allowed the optical length of the FP cavities to remain stable enough. The intensity of transmitted light from the FP cavities also remains stable. These home-made systems are simple, convenient, and reliable. Our FP cavities always transmit on-resonance  $l = 3$  mode but reflect other off-resonance modes. The cyclic transformation module in the experimental setup does not need to be optimized for each incident OAM mode.

Since the FP cavity is a single transparent crystal, it is not possible to scan the length of the FP cavity by attaching a piece of piezoelectric ceramic. Therefore, we place a photodetector

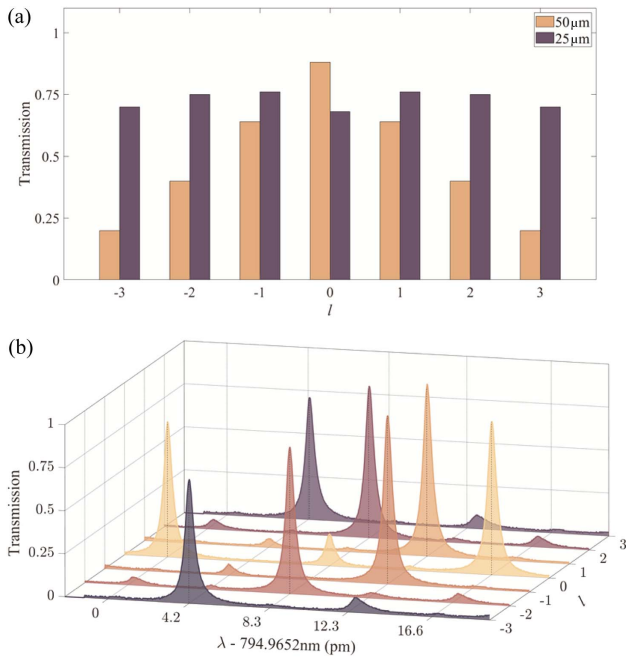


**Fig. 3.** Measured transmissions for the FP1. (a) Transmissions of the FP1 cavity for different  $l$  modes for a 50  $\mu\text{m}$  and 25  $\mu\text{m}$  incident beam waist, respectively. (b) Transmission spectra of different  $l$  modes through FP1. The wavelength interval between the two main peaks in the  $l = 0$  mode means the free spectral range (FSR) of the cavity. The transmission spectra for paired modes  $l = \pm 1, \pm 2,$  and  $\pm 3$  are almost identical because the FP1 cavity cannot distinguish the  $+$  and  $-l$  modes.

behind the FP1 cavity and scan the wavelength of the laser to obtain a functional relationship between the transmission of the FP1 cavity and the wavelength of the laser; the experimental results are depicted in Fig. 3(b).

The experimental data for the FP1 cavity are free spectral range  $\text{FSR} = 7.90$  GHz, bandwidth  $\Delta\omega = 287$  MHz, finesse  $F = 27.4$ , and beam waist  $w_0 = 50$   $\mu\text{m}$ . The theoretical data are  $\text{FSR} = 8.57$  GHz,  $\Delta\omega = 287$  MHz,  $F = 29.9$ , and  $w_0 = 55$   $\mu\text{m}$ . The experimental and theoretical results are reasonably consistent. Experimentally, in order to increase transmission of FP1 cavity in the  $l = \pm 3, p = 0$  modes, we

reduced the beam waist of the incident light beam to half of that of the cavity mode ( $w_0 = 50$   $\mu\text{m}$ ) and observed a significant enhancement of transmission in the  $l = \pm 3$  modes behind the FP1 cavity. This also led to mode mismatch between the mode of the incident beam and mode of the FP1 cavity; for example, a small peak appeared in the middle of two large peaks when the incident beam was in the  $l = 0$  mode. In addition, at the wavelength  $\lambda = 794.9694$  nm, the small transmission peaks appeared in the  $l = \pm 1$  modes due to the presence of the  $p = 1$  component in the vortex beams produced through the QP, which also satisfied the resonance condition of the cavity in the  $l = \pm 3, p = 0$  modes.

Due to experimental constraints, we are only able to modulate the phase of the incident light beam leading to the emergence of higher-order radial modes ( $p \neq 0$ ) in the vortex beam. On the one hand, we narrow the incident beam waist to reduce the weighting of the higher-order radial modes. This method improves the transmission of the  $p = 0$  mode but also generates mode mismatch between the input mode and the cavity mode; on the other hand, the generation of higher-order radial modes also leads to degeneracy of multiple OAM modes at the resonance point of the FP cavity. If the phase and amplitude of the incoming light beam can be modulated simultaneously, for instance, by using spatial light modulator (SLM) [35], it is anticipated to achieve a perfect OAM-mode separation for FP cavities.

Our FP cavities can discriminate four cases for  $|l| = 0, 1, 2, 3$ . Thus, the cyclic transformation device only works in six modes  $\{l = -3, -2, -1, 0, 1, 2\}$ . Experimentally we send each of the six OAM modes into the cyclic transformation device for testing one by one. For each input mode, each output mode after undergoing the cyclic transformation implemented projective measurement with a combination of QP and single-mode fiber, and a total of 36 measurements were completed. Figure 4(a) shows the experimental results; the distinct peaks imply that each input mode moved to the correct output mode after a cyclic transformation.

For a selected input mode, the efficiency  $E$  of the correct output mode after the cyclic transformation is shown in Fig. 4(b). The efficiency  $E = I_c/I_{\text{total}}$  means the probability that the correct mode is created [18].  $I_c$  is the power of the correctly created mode, and  $I_{\text{total}} = \sum_{l=-3}^{+2} I_l$  is the sum of the intensity collected at all six collected output modes.

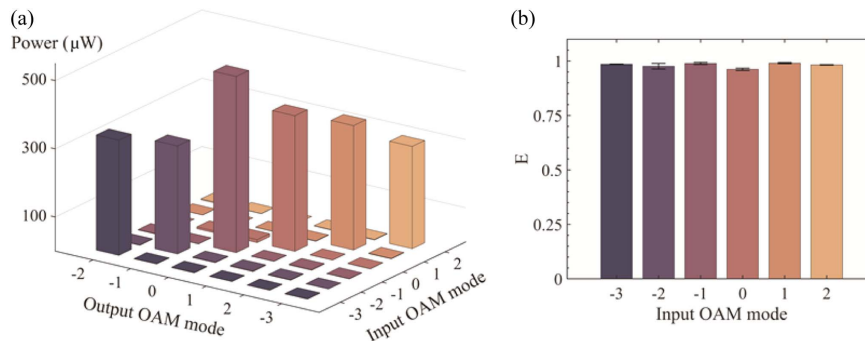


**Fig. 4.** Experimental results for six-mode cyclic transformation. (a) Measured power of six output OAM modes for six input OAM modes. Each color represents a specific input mode. (b) Measured efficiency  $E$  for a different input mode.

The measured results clearly show that our six-mode cyclic transformation operation has a high efficiency, with an average efficiency greater than 96%.

The average efficiency depends mainly on the transmittance and reflectance of the FP cavity to the OAM modes. The discrepancy of our measurement from the ideal cyclic transformation is mainly attributed to the mode mismatch between the resonant OAM modes and the cavity. If we replace the Q-plates by SLMs that realize amplitude-phase modulation, the OAM modes will always remain at high purity as the azimuthal mode indices  $l$  increase. It is anticipated that the transmittance of the FP1 cavity will be further improved in this mode.

Experimentally, since our FP cavities are flat-convex cavities, as a result, the transverse modes of the vortex beam from the convex side of the FP2 cavity are poor relative to that of the planar side. This deformation of the transverse modes also leads to a decrease in the collection efficiency of the single-mode fiber, which in turn reduces the average efficiency. A possible solution is to build a normal FP cavity utilizing two flat-concave mirrors and a piece of piezoelectric ceramic attached to one of the two separated mirrors, so that the distortion of the transverse OAM mode is suppressed. In addition, the coupling efficiency of the high-order modes is generally lower than that of the low-order modes in the phase-flattening technology, which is also reflected in our experimental results [36].

Furthermore, we discuss the feasibility of our current experimental setup in the quantum regime. The ideal quantum Pauli-X gate requires that the incident single photons are a quantum superposition of different OAM states with equal probability amplitudes. After a cyclic transformation operation, the output single photons remain in this quantum superposition state and the relative phase of the superposition states remains constant. A phase-locking system is required to lock the phase difference between the transmitted and reflected fields of the nonreciprocal MZI in order to ensure that the relative phase of the output quantum superposition state is fixed. The photons passing through the FP cavity have a long survival time. In order to achieve stable interference between the transmitted and reflected fields, it is also necessary to input single-photon pulses with narrow bandwidth and long coherence length matching the FP cavity. The coherence length is estimated to be about  $20FL$ , where  $F$  and  $L$  are the finesse and optical

length of the FP cavity, respectively.  $2FL$  is the distance of one round trip of the photons in the FP cavity. The coherence length of  $20FL$  can ensure that the photons overlap each other. It remains constant if the cavity linewidth is fixed.

To summarize, the factors affecting the fidelity of high-dimensional single-photon quantum Pauli-X gate are mainly the transmittance and reflectance of the FP cavity to the OAM modes, the accuracy of the MZI-controlled phases, and the efficiency of projective measurements on the OAM modes and their superpositions. Thus, the average efficiency is the one that will affect the fidelity of the gate.

Finally, we discuss the scalability of our system to higher dimensions. For a vortex beam with  $2l$  modes  $\{-(l+1), -l, \dots, l\}$ , the cyclic transformation can be achieved by adjusting the lengths of the FP1 and FP2 cavities so that they satisfy the resonance condition of the  $(l+1)$  mode. The maximum number of supportable OAM modes  $N_{\max}$  depends only on the number of modes  $l$  that the FP cavity can distinguish. To be more specific, we introduce  $\Delta\nu_{\max}$  as the spectral width of the peak for each cavity mode when the transmission decreases to 0.5% of the amplitude. In this case the gate errors caused by the spectral overlap between cavity modes with different  $l$  is negligible. Then the number of supportable modes is proportional to the finesse of the cavity, given by  $N_{\max} = \text{FSR}/\Delta\nu_{\max} \propto F$ .

Thus, to increase the maximum number of distinguishable OAM modes in the cavity, we can increase the reflectivity  $R$  of the two identical mirrors of the FP cavity. As shown in Fig. 5(a), the finesse of the FP cavity increases exponentially with the increasing reflectivity  $R$  of the two mirrors. Simultaneously, the cavity length should be shortened such that the cavity linewidth is unchanged; see Fig. 5(b). This approach enables our system to extend to very high dimensions without requiring additional optical components [37,38].

Experimentally, the number of OAM modes that our system can accommodate is constrained by the length of the FP cavity. For a rough estimation, the minimum cavity length is about 1 mm by using the same technology making our cavity. For a cavity linewidth of 55.3 MHz, the reflectivity of both mirrors is  $R = 99.5\%$ , resulting in  $F = 943$ , as indicated by the blue dots in Figs. 5(a) and 5(b). In this case  $N_{\max} \approx 68$ , and the corresponding highest dimension  $d_{\max} = 2(N_{\max} - 1) \approx 134$  for the gate is available. The average efficiency relies on the

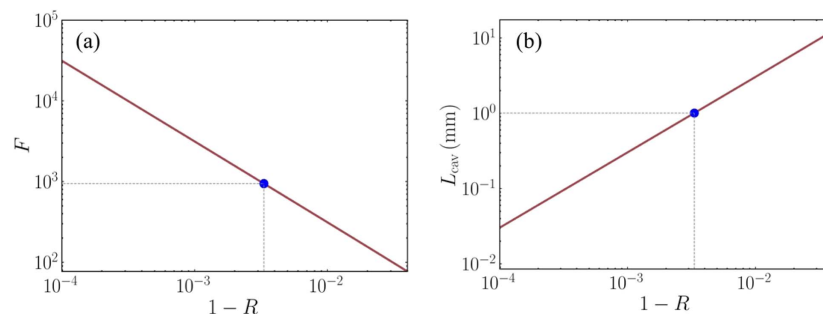


**Fig. 5.** (a) Finesse of the cavity as a function of mirror reflectivity  $R$ . (b) Cavity length as a function of the mirror reflectivity  $R$ , where we have kept a constant cavity linewidth. The blue dots in (a) and (b) represent the case when the cavity length is set to be 1 mm, which is accessible in experiment, and the corresponding finesse is  $F = 943$ .

transmittance and reflectance of the FP cavity to the OAM modes. Notably, the average efficiency remains stable even as the system scales to higher dimensions. If a shorter cavity length of 0.1 mm is applied [39], the cyclic transformation can be extended to  $N_{\max} \approx 700$  when  $R = 99.9\%$ .

## 5. CONCLUSIONS

By simply using the FP cavities, the optical circulators, and a topological charge flipper, we have experimentally demonstrated the six-mode cyclic transformation with an average efficiency exceeding 96%. By further improving the fineness of the FP cavity and using an amplitude-phase modulator [35], it is feasible to achieve cyclic transformations for more OAM modes. If the phase of the MZI can be stabilized at a level of about one tenth of the wavelength and single photons with narrow linewidth and long coherence length can be incident, our method can also be straightforwardly used for conducting a high-dimensional quantum Pauli-X gate. Thus, this work provides a building block for high-dimensional quantum information processing.

**Funding.** Innovation Program for Quantum Science and Technology (2021ZD0301400); National Natural Science Foundation of China (92365107, 12305020, 12334012); National Key Research and Development Program of China (2019YFA0308700, 2019YFA0308704, 2022YFA1405000); Program for Innovative Talents and Teams in Jiangsu (JSSCTD202138); Natural Science Foundation of Jiangsu Province, Major Project (BK20212004); China Postdoctoral Science Foundation (2023M731613); Jiangsu Funding Program for Excellent Postdoctoral Talent (2023ZB708).

**Acknowledgment.** The authors thank Prof. Xi-Lin Wang, Pei Wan, and Yi-Peng Zhang for their helpful discussions.

**Disclosures.** The authors declare that they have no conflicts of interest.

**Data Availability.** Data underlying the results presented in this paper are not publicly available at this time but may be obtained from the authors upon reasonable request.

## REFERENCES

1. L. Allen, M. W. Beijersbergen, R. J. C. Spreeuw, *et al.*, "Orbital angular momentum of light and the transformation of Laguerre-Gaussian laser modes," *Phys. Rev. A* **45**, 8185–8189 (1992).
2. G. Gibson, J. Courtial, M. J. Padgett, *et al.*, "Free-space information transfer using light beams carrying orbital angular momentum," *Opt. Express* **12**, 5448–5456 (2004).
3. J. Wang, J.-Y. Yang, I. M. Fazal, *et al.*, "Terabit free-space data transmission employing orbital angular momentum multiplexing," *Nat. Photonics* **6**, 488–496 (2012).
4. M. Krenn, R. Fickler, M. Fink, *et al.*, "Communication with spatially modulated light through turbulent air across Vienna," *New J. Phys.* **16**, 113028 (2014).
5. A. Sit, F. Bouchard, R. Fickler, *et al.*, "High-dimensional intracity quantum cryptography with structured photons," *Optica* **4**, 1006–1010 (2017).
6. S.-S. Liu, Y.-B. Lou, and J.-T. Jing, "Orbital angular momentum multiplexed deterministic all-optical quantum teleportation," *Nat. Commun.* **11**, 3875–3882 (2020).
7. Y.-B. Lou, Y.-H. Lv, J.-B. Wang, *et al.*, "Orbital angular momentum multiplexed deterministic all-optical quantum erasure-correcting code," *Phys. Rev. Lett.* **132**, 040601 (2024).
8. S.-S. Liu, Y.-H. Lv, X.-T. Wang, *et al.*, "Deterministic all-optical quantum teleportation of four degrees of freedom," *Phys. Rev. Lett.* **132**, 100801 (2024).
9. A. C. Dada, J. Leach, G. S. Buller, *et al.*, "Experimental high-dimensional two-photon entanglement and violations of generalized Bell inequalities," *Nat. Phys.* **7**, 677–680 (2011).
10. R. Fickler, R. Lapkiewicz, W. N. Plick, *et al.*, "Quantum entanglement of high angular momenta," *Science* **338**, 640–643 (2012).
11. M. Krenn, M. Huber, R. Fickler, *et al.*, "Generation and confirmation of a (100×100)-dimensional entangled quantum system," *Proc. Natl. Acad. Sci. USA* **111**, 6243–6247 (2014).
12. R. Fickler, G. Campbell, B. Buchler, *et al.*, "Quantum entanglement of angular momentum states with quantum numbers up to 10,010," *Proc. Natl. Acad. Sci. USA* **113**, 13642–13647 (2016).
13. S.-L. Liu, Z.-Y. Zhou, S.-K. Liu, *et al.*, "Coherent manipulation of a three-dimensional maximally entangled state," *Phys. Rev. A* **98**, 062316 (2018).
14. B. C. Hiesmayr, M. J. A. de Dood, and W. Löffler, "Observation of four-photon orbital angular momentum entanglement," *Phys. Rev. Lett.* **116**, 073601 (2016).
15. M. Malik, M. Erhard, M. Huber, *et al.*, "Multi-photon entanglement in high dimensions," *Nat. Photonics* **10**, 248–252 (2016).
16. X.-L. Wang, Y.-H. Luo, H.-L. Huang, *et al.*, "18-qubit entanglement with six photons' three degrees of freedom," *Phys. Rev. Lett.* **120**, 260502 (2018).
17. J. Courtial and M. J. Padgett, "Performance of a cylindrical lens mode converter for producing Laguerre-Gaussian laser modes," *Opt. Commun.* **159**, 13–18 (1999).
18. F. Schlederer, M. Krenn, R. Fickler, *et al.*, "Cyclic transformation of orbital angular momentum modes," *New J. Phys.* **18**, 043019 (2016).
19. A. Babazadeh, M. Erhard, F.-R. Wang, *et al.*, "High-dimensional single-photon quantum gates: concepts and experiments," *Phys. Rev. Lett.* **119**, 180510 (2017).
20. F. Brandt, M. Hiekkamäki, F. Bouchard, *et al.*, "High-dimensional quantum gates using full-field spatial modes of photons," *Optica* **7**, 98–107 (2020).
21. A. Asadian, P. Erker, M. Huber, *et al.*, "Heisenberg-Weyl Observables: Bloch vectors in phase space," *Phys. Rev. A* **94**, 010301 (2016).
22. N. González, G. Molina-Terriza, and J. P. Torres, "How a Dove prism transforms the orbital angular momentum of a light beam," *Opt. Express* **14**, 9093–9102 (2006).
23. J. Leach, M. J. Padgett, S. M. Barnett, *et al.*, "Measuring the orbital angular momentum of a single photon," *Phys. Rev. Lett.* **88**, 257901 (2002).
24. J. Leach, J. Courtial, K. Skeldon, *et al.*, "Interferometric methods to measure orbital and spin, or the total angular momentum of a single photon," *Phys. Rev. Lett.* **92**, 013601 (2004).
25. W.-H. Zhang, Q.-Q. Qi, J. Zhou, *et al.*, "Mimicking faraday rotation to sort the orbital angular momentum of light," *Phys. Rev. Lett.* **112**, 153601 (2014).
26. X.-Q. Gao, M. Krenn, J. Kysela, *et al.*, "Arbitrary d-dimensional Pauli X gates of a flying qudit," *Phys. Rev. A* **99**, 023825 (2019).
27. G. C. G. Berkhout, M. P. J. Lavery, J. Courtial, *et al.*, "Efficient sorting of orbital angular momentum states of light," *Phys. Rev. Lett.* **105**, 153601 (2010).
28. M. Mirhosseini, M. Malikt, Z.-M. Shi, *et al.*, "Efficient separation of the orbital angular momentum eigenstates of light," *Nat. Commun.* **4**, 2781–2786 (2013).
29. Y.-H. Wen, I. Chremmos, Y.-J. Chen, *et al.*, "Spiral transformation for high-resolution and efficient sorting of optical vortex modes," *Phys. Rev. Lett.* **120**, 193904 (2018).
30. S.-B. Wei, S. K. Earl, J. Lin, *et al.*, "Active sorting of orbital angular momentum states of light with a cascaded tunable resonator," *Light Sci. Appl.* **9**, 10 (2020).

31. L. Marrucci, C. Manzo, and D. Paparo, "Optical spin-to-orbital angular momentum conversion in inhomogeneous anisotropic media," *Phys. Rev. Lett.* **96**, 163905 (2006).
32. B. Sephton, A. Dudley, and A. Forbes, "Revealing the radial modes in vortex beams," *Appl. Opt.* **55**, 7830–7835 (2016).
33. E. Karimi, G. Zito, B. Piccirillo, *et al.*, "Hypergeometric-Gaussian modes," *Opt. Lett.* **32**, 3053–3055 (2007).
34. H. Sroor, Y.-W. Huang, B. Sephton, *et al.*, "High-purity orbital angular momentum states from a visible metasurface laser," *Nat. Photonics* **14**, 498–504 (2020).
35. V. Arrizón, U. Ruiz, R. Carrada, *et al.*, "Pixelated phase computer holograms for the accurate encoding of scalar complex fields," *J. Opt. Soc. Am. A* **24**, 3500–3507 (2007).
36. H. Qassim, F. M. Miatto, J. P. Torres, *et al.*, "Limitations to the determination of a Laguerre–Gauss spectrum via projective, phase-flattening measurement," *J. Opt. Soc. Am. B* **31**, A20–A23 (2014).
37. S. Goel, S. Leedumrongwatthanakun, N. H. Valencia, *et al.*, "Inverse design of high-dimensional quantum optical circuits in a complex medium," *Nat. Phys.* **20**, 232–239 (2024).
38. J.-W. Wang, F. Sciarrino, A. Laing, *et al.*, "Integrated photonic quantum technologies," *Nat. Photonics* **14**, 273–284 (2020).
39. Y.-X. Liu, Z.-H. Wang, P.-F. Yang, *et al.*, "Realization of strong coupling between deterministic single-atom arrays and a high-finesse miniature optical cavity," *Phys. Rev. Lett.* **130**, 173601 (2023).